IEICE TRANS. ELECTRON., VOL.E104–C, NO.10 OCTOBER 2021

INVITED PAPER *Special Section on Microwave and Millimeter-Wave Technologies*

Linearization Technologies for High Efficiency Power Amplifier of Cellular Base Stations

Yasunori SUZUKI[†a)] ***and*** **Shoichi NARAHASHI**[††], ***Senior Members***

SUMMARY This paper presents linearization technologies for high efficiency power amplifiers of cellular base stations. These technologies are important to actualizing highly efficient power amplifiers that reduce power consumption of the base station equipment and to achieving a sufficient non-linear distortion compensation level. It is well known that it is very difficult for a power amplifier using linearization technologies to achieve simultaneously high efficiency and a sufficient non-linear distortion compensation level. This paper presents two approaches toward addressing this technical issue. The first approach is a feed-forward power amplifier using the Doherty amplifier as the main amplifier. The second approach is a digital predistortion linearizer that compensates for frequency dependent intermodulation distortion components. Experimental results validate these approaches as effective for providing power amplification for base stations.

key words: *feed-forward, predistortion, power amplifier, cellular base station*

1. Introduction

Mobile communication systems have continuously evolved to attain new features and to provide new services such as voice communications and moving picture streaming. First-generation (1G) and second-generation (2G) mobile communication systems provide voice communications using a narrow bandwidth in the 800-MHz band [1], [2]. Third-generation (3G) mobile communication systems support video communications and employ new frequency bands such as the 2-GHz band. Fourth-generation (4G) mobile communication systems can offer many application services for smart phones. In 2020, fifth-generation (5G) mobile communication systems launched commercial services in Japan [3]. Many use-case scenarios provided by 5G mobile communication systems are for industry, medical services, consumer electronics, and so on.

A power amplifier (PA) for cellular base stations is a key device in the deployment of mobile communication systems, and technical progress in PAs has contributed to improving the performance of base station equipment.

The base station PA for 1G mobile communication systems employs a saturated-type PA. The modulation scheme and multiplexing scheme of 1G mobile communication systems use frequency modulation and frequency division multiple access. The base station has many saturated-type PAs corresponding to the number of radio frequencies.

The base station PA for 2G mobile communication systems employs a linear PA using a feed-forward power amplifier (FFPA) [4]. The base station PA needs to amplify multiple radio frequencies. In this case, the PA generates intermodulation distortion (IMD) components between multiple radio frequencies [5]. If the PA is designed using the back-off method, the saturated output power level of the PA is determined to be in the class of several kilowatts (kW). The FFPA provides superior IMD component cancellation, while the saturated output power level of the PA is approximately in the 200W class. Therefore, it is indispensable for the base station PA to compensate for these IMD components. The FFPA also enables downsizing of the base station equipment.

The FFPA has become very well known due to Seidel's paper [6]. Although the FFPA has superior IMD component cancellation, it is very difficult to maintain the cancellation conditions. This technical issue is well addressed using pilot signals. Noijma and Narahashi developed a self-adjusting FFPA (SAFF) for the PA used in the Personal Digital Cellular (PDC) base station [7]. Employing the SAFF yields a miniaturized base station for installation in buildings, and a higher degree of flexibility in the deployment of PDC base stations.

The base station equipment for 3G mobile communication systems comprises a PA and digital predistortion linearizer (DPDL) [8]. The DPDL uses a digital signal processing unit, but does not require complicated circuits such as for the FFPA. Therefore, the DPDL has advantages in terms of manufacturing cost and size compared to the FFPA. These linearization technologies, DPDL and FFPA, mainly focus on lower IMD components for achieving adjacent channel leakage power ratio (ACLR) specifications [2], [3]. The next challenge for these linearization technologies is to reduce the power consumption of the base station equipment. In general, the PA consumes a major part of the power supply of the base station equipment. However, the PA can reduce power consumption operating near the saturation output power region, but the PA generates higher level and more complicated IMD components that are frequency dependent [9], [10].

The conventional DPDL cannot sufficiently compensate for these IMD components, while the conventional FFPA cannot reduce the power consumption of the base station PA. A technical breakthrough is needed for the FFPA

Manuscript received January 20, 2021.
Manuscript revised February 26, 2021.
Manuscript publicized March 24, 2021.

[†]The author is with NTT DOCOMO, INC., Yokosuka-shi, 239–8536 Japan.
[††]The author is with Setsunan University, Neyagawa-shi, 572–8508 Japan.
a) E-mail: yasunori.suzuki.ws@nttdocomo.com

DOI: 10.1587/transele.2021MMI0009

Copyright © 2021 The Institute of Electronics, Information and Communication Engineers

and DPDL.

This paper presents linearization technologies that offer high efficiency amplification of the PA. There are two approaches. The first is an FFPA using the Doherty amplifier [11]–[13] as the main amplifier [14]. The Doherty amplifier extends the saturation output power region. Based on this feature, it can reduce the output back-off level of the main amplifier by the maximum of 6 dB. An FFPA employing the Doherty amplifier as the main amplifier can improve efficiency. The second approach is a DPDL employing a frequency characteristic compensator that compensates for the complicated IMD components [15]–[17]. The frequency characteristic compensator is a kind of filter for equalizing the frequency characteristics of the IMD components. The PA can operate near the saturation output power region when employing the DPDL with the frequency characteristic compensator. These approaches are the first fundamental investigation for reducing the power consumption of the base station equipment. This paper presents the concepts behind these linearization technologies and fundamental investigation results that validate the effectiveness of the base station PA.

2. Feed-Forward Power Amplifier Using Doherty Amplifier

2.1 Principle

Figure 1 shows the basic configuration of a FFPA comprising a distortion detection loop and distortion cancellation loop. The distortion detection loop comprises a power divider, variable attenuator, phase shifter, main amplifier, delay line, and power combiner and divider. The distortion cancellation loop comprises a power combiner and divider, delay line, variable attenuator, phase shifter, error amplifier, and power combiner.

In the distortion detection loop, the vector regulator that consists of the variable attenuator and phase shifter adjusts the amplitude and phase values to suppress the transmitted signal that is forwarded to the vector regulator of the distortion cancellation loop. The vector regulator of the distortion cancellation loop adjusts the amplitude and phase values to suppress the distortion component at the output port of the power divider. In order to understand more easily these operations, spectrum images are also shown in Fig. 1.

It is very well known that making these adjustments is very difficult to maintain the suppression level of a transmitted signal or distortion components because of temperature changes. The SAFF can completely provide a sufficient suppression level using pilot signals whether or not the temperature changes.

The efficiency of the FFPA is expressed as

$$\eta_T = \frac{P_{out}}{P_{DC\_M} + P_{DC\_A}}, \tag{1}$$

where P_{DC_M} and P_{DC_A} are the power supply of the main amplifier and error amplifier, respectively. Term P_{out} is the output power of the FFPA and is given as

$$P_{out} = \frac{P_{out\_M}}{L} + \frac{P_{out\_A}}{C_A}, \tag{2}$$

where P_{out_M} and P_{out_A} are the output power of the main amplifier and error amplifier, respectively. Term L is the insertion loss from the output terminal of the main amplifier to that of the FFPA. Term C_A is the coupling factor from the output terminal of the error amplifier to that of the FFPA. The drain efficiency, η_{d_m}, of the main amplifier and the drain efficiency, η_{d_A}, of the error amplifier are respectively defined as

$$\eta_{d\_M} = \frac{P_{out\_M}}{P_{DC\_M}} \quad \text{and} \tag{3}$$

$$\eta_{d\_A} = \frac{P_{out\_A}}{P_{DC\_A}}. \tag{4}$$

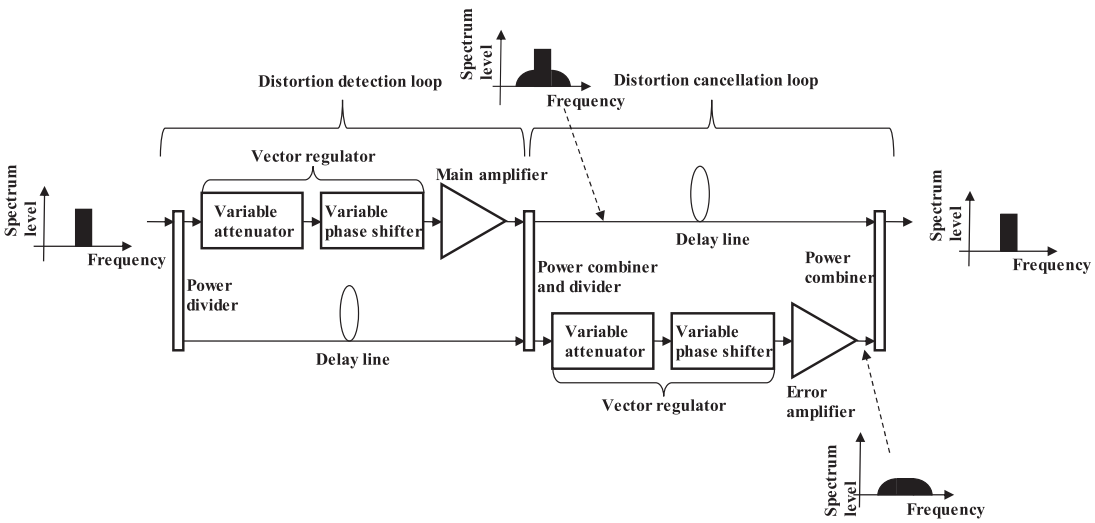

Fig. 1 Basic configuration of FFPA.

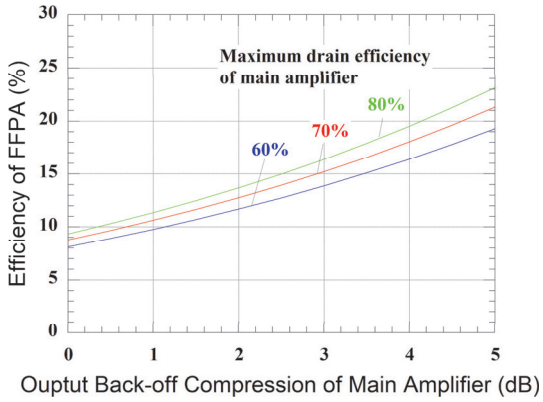

Fig. 2 Calculation results of FFPA efficiency.

From these equations, η_T, is given by

$$\eta_T = \frac{1}{L}\frac{\eta_{d\_M}}{1+\frac{P_{out\_A}}{P_{out\_M}}\frac{\eta_{d\_M}}{\eta_{d\_A}}} + \frac{1}{C_A}\frac{\eta_{d\_A}}{1+\frac{P_{out\_M}}{P_{out\_A}}\frac{\eta_{d\_A}}{\eta_{d\_M}}}. \quad (5)$$

In general, the main amplifier is under a Class-AB bias condition, while the error amplifier is under a Class-A bias condition [18], [19]. To improve efficiency η_T, the FFPA requires a Class-B main amplifier. Therefore, the main amplifier is set to a Class-B bias condition, while the error amplifier is set to a Class-A bias condition. The drain efficiencies, η_{d_m} and η_{d_A}, are expressed in terms of the maximum drain efficiency and output back-off as

$$\eta_{d\_M} = \frac{\eta_{d\_M\_max}}{\sqrt{10^{\frac{B_M}{10}}}} \quad \text{and} \quad (6)$$

$$\eta_{d\_A} = \frac{\eta_{d\_A\_max}}{10^{\frac{B_A}{10}}}, \quad (7)$$

where $\eta_{d\_M\_max}$ and $\eta_{d\_A\_max}$ are the maximum drain efficiencies of the main amplifier and error amplifier, respectively. Terms B_M and B_A are the output back-off from the saturation output power of the main amplifier and error amplifier, respectively.

Figure 2 shows the calculation results on the FFPA efficiency using (5). The FFPA efficiency is represented on the horizontal axis. The output back-off compression of the main amplifier is represented on the vertical axis. The main amplifier and error amplifier are under Class-B and Class-A bias conditions, respectively. The other parameters for (5) are the same as those for the FFPAs for cellular base stations [7], [18], [19]. The maximum drain efficiencies of the main amplifier are set to 60%, 70%, and 80%.

The output back-off compression of 0 dB shown in Fig. 2 represents the output back-off level of the main amplifier with typical parameters. In this case, the efficiency of the FFPA is approximately 8% at the maximum drain efficiency of 70% and the output back-off compression of 0 dB. If the output back-off compression becomes 3 dB, the efficiency of the FFPA becomes approximately 16% at the maximum drain efficiency of the main amplifier of 70%.

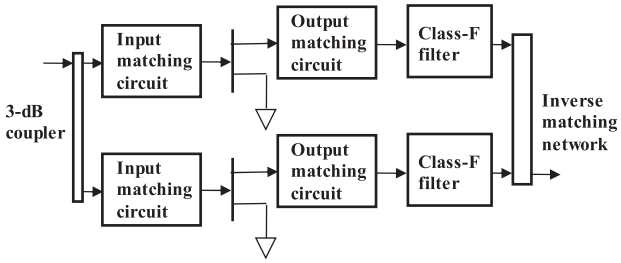

Fig. 3 Basic configuration of Class-F Doherty amplifier.

Figure 2 shows that it is very important to reduce the output back-off of the main amplifier in order to improve the efficiency of the FFPA. Moreover, if the maximum drain efficiency of the main amplifier improves from 70% to 80%, the efficiency of the FFPA increases from 1 percentage point to 2 percentage point. In order to improve the drain efficiency of the FFPA, it is important to increase the maximum drain efficiency of the main amplifier. For these reasons, increasing the maximum drain efficiency is indispensable to the main amplifier in order to reduce the output back-off level.

2.2 Configurations

Figure 3 shows the configuration of the Doherty amplifier using a Class-F filter [14]. The Doherty amplifier was proposed by W.H. Doherty [11]. The Doherty amplifier comprises a carrier amplifier and peaking amplifier. The Class-F Doherty amplifier shown in Fig. 3 employs Class-F filter circuits at the output side of the output matching circuits [20]. The Class-F Doherty amplifier reduces the output back-off level compared to that for the Class-B amplifier. For this reason, we employ the Class-F Doherty amplifier as the main amplifier of the FFPA.

2.3 Experimental Results

We fabricated a 2-GHz band 1W class FFPA using a Class-F Doherty amplifier and Class-B main amplifier [14]. The fabricated Class-B main amplifier comprises input and output matching circuits to maximize the efficiency. These amplifiers employ commercially available GaAs metal-semiconductor filed-effect transistors (MESFETs). The power divider in Fig. 1 employs a 3-dB directional coupler. The power combiner and divider employ a 49-dB directional coupler. The power combiner employs a 10-dB directional coupler.

Figure 4 shows the drain efficiency performance of the fabricated Class-F Doherty amplifier and Class-B main amplifier. The measurement frequency is 2.14 GHz. The test signal is a continuous wave (CW). The maximum drain efficiency of the Class-F Doherty amplifier and Class-B main amplifier are approximately 70%. The drain efficiency of the Class-F Doherty amplifier can maintain a level higher than 58% when the output back-off from the saturation output power is from 0 dB to 6 dB. On the other hand, the drain

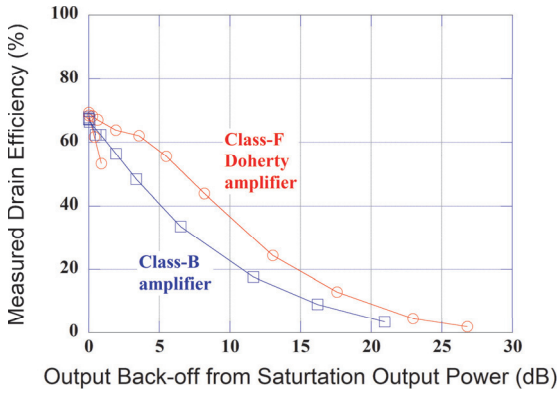

Fig. 4 Drain efficiency performance of Class-F Doherty amplifier and Class-B conventional amplifier.

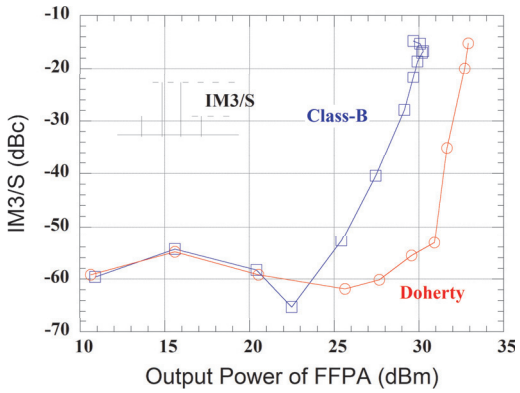

Fig. 6 Experimental results of IM3/S performance of FFPA with Class-F Doherty amplifier and the conventional FFPA.

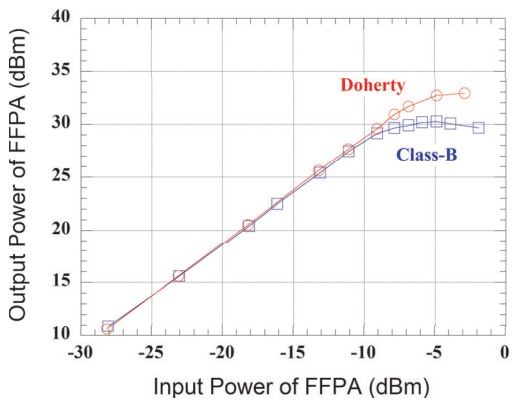

Fig. 5 Output power performance of FFPA with Class-F Doherty amplifier.

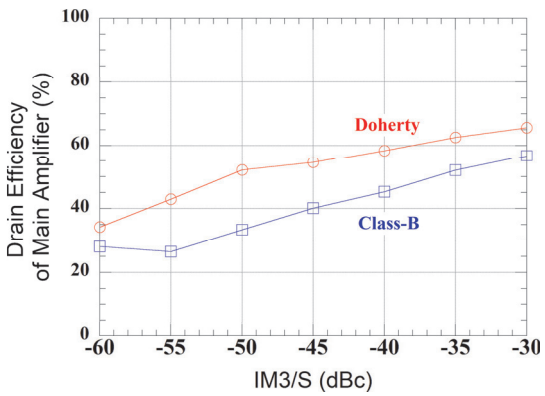

Fig. 7 Drain efficiency of main amplifier vs. IM3/S.

efficiency of the Class-B main amplifier can maintain a level higher than 38% under the same conditions. From the experimental results, the Class-F Doherty amplifier achieves a higher drain efficiency compared to that for the Class-B main amplifier.

Figure 5 shows the output power performance of the FFPA with the Class-F Doherty amplifier and Class-B main amplifier. The measurement frequency is 2.14 GHz. The test signal is a CW. The output power of the FFPA with the Class-F Doherty amplifier and Class-B main amplifier is represented on the vertical axis. The input power of the FFPA with the Class-F Doherty amplifier and Class-B main amplifier is represented on the horizontal axis. The gain of the FFPA with the Class-F Doherty amplifier and Class-B main amplifier are 38 dB. The saturation output power of the FFPA with the Class-F Doherty amplifier achieves 33 dBm, while that of the FFPA with the Class-B main amplifier is 30 dBm. This is because the Class-F Doherty amplifier has the peaking amplifier.

Figure 6 shows the third-order IMD performance of the FFPA with the Class-F Doherty amplifier and Class-B main amplifier. The test signal comprises two CWs that have identical amplitudes and frequencies of 2.140 GHz and 2.141 GHz. The power ratio of the third-order IMD component to signal component (hereinafter IM3/S) is represented on the vertical axis. The output power of the FFPA with the Class-F Doherty amplifier and Class-B main amplifier is represented on the horizontal axis. The IM3/S of the FFPA with the Class-F Doherty amplifier is −50 dBc at the output power of 31 dBm. The IM3/S of the FFPA with the Class-B main amplifier is −50 dBc at the output power of 26 dBm. The FFPA with the Class-F Doherty amplifier can improve the output power by 5 dB at the IM3/S of −50 dBc.

When the output powers of the FFPA with the Class-F Doherty amplifier and Class-B main amplifier are 30 dBm, the IM3/S of the FFPA with the Class-F Doherty amplifier is lower than that for the FFPA with the Class-B main amplifier by approximately 32 dB. The IM3/S of the FFPA with the Class-F Doherty amplifier slightly improves compared to that with the Class-B main amplifier. This seems to be because the Class-F filter and Doherty amplifier configuration is used. The Class-F filter provides second-order harmonic tuning to suppress the third-order IMD components. Another reason to use this configuration is to expand the power of the output signal of the carrier amplifier using the peaking amplifier. However, these are only hypotheses. They must be validated through further numerical analysis and experiments. Based on the experimental results, the FFPA with the Class-F Doherty amplifier reduces the IM3/S.

Figure 7 shows the improvement in the drain efficiency

of the main amplifier. The drain efficiency of the main amplifier is represented on the vertical axis. The IM3/S values are represented on the horizontal axis. The test signal is the same as that in Fig. 6. The open circles represent the experimental results of the FFPA with the Class-F Doherty amplifier, while the open squares represent that of the FFPA with the Class-B main amplifier. The main amplifier with the Class-F Doherty amplifier achieves higher efficiency than that with the Class-B amplifier. This is because the drain efficiency of the main amplifier with the Class-F Doherty amplifier improves the efficiency. The main amplifier with the Class-F Doherty amplifier extends the drain efficiency by 20 percentage points at the IM3/S of −50 dBc.

Based on these experimental results, the FFPA with the Class-F Doherty amplifier as the main amplifier improves the efficiency when the IM3/S is the same level.

3. Digital Predistorter Compensating Frequency Dependent IMD Components

3.1 Principle

Figure 8 shows the basic configuration of the DPDL compensating for the frequency dependent IMD components including the PA [21].

The DPDL comprises the i_{th}-order distortion generator, i_{th}-order vector regulator, i_{th}-order frequency characteristic compensator, a controller, and monitor. The DPDL is based on a power-series model.

Figure 9 shows the parameter setting procedure of the vector regulator and frequency characteristic compensator. Figure 9 (a) shows the output spectrum of a PA without compensation signals. The frequency is represented on the horizontal axis. The spectrum level is represented on the vertical axis. Because the output spectrum components have different amplitude and phase values, the output spectrum components shown in Fig. 9 (a) are illustrated using the I-Q plane. Figure 9 (b) shows the output spectrum of the PA with the vector regulator only. If the vector regulator sets the vector value for the lower IMD component, the DPDL cannot cancel an upper IMD component with different phase and amplitude values. Figure 9 (c) shows the output spectrum of the PA with a frequency characteristic compensator. The frequency characteristic compensator can set the optimum amplitude and phase values. Therefore, the DPDL with the frequency characteristic compensator can cancel lower and upper IMD components with different amplitude and phase values.

Figure 10 shows the experimental results using three CWs that have identical amplitude values with different frequencies. The output level is represented on the vertical axis. The frequency with the center frequency of 2 GHz and the bandwidth of 60 MHz is represented on the horizontal axis. The three-tone signal is up-converted by the vector signal generator to a frequency at 1.992 GHz, 1.994 GHz, and 2.002 GHz. The PA offers 1W output power in the 2-GHz band. The PA uses commercially available GaAs MESFETs. The bias condition is set to Class-A. The output back-off is set to 3 dB from a 1-dB gain compression point as measured with a single tone. Figure 10 (a) shows the output component level without the DPDL. The open circles represent the third-order IMD components. The open squares represent the fifth-order IMD components.

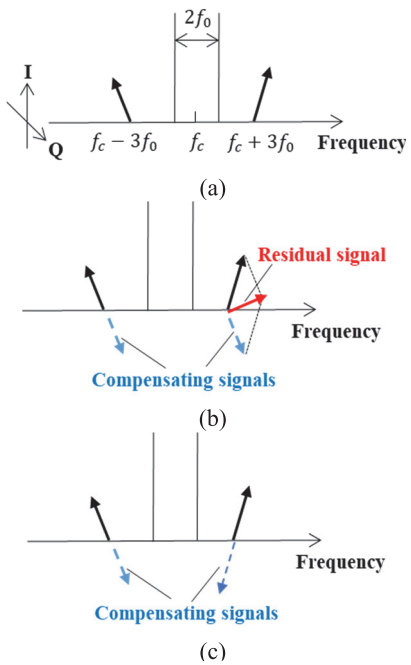

Fig. 9 Parameter setting procedure of DPDL compensating frequency dependent IMD components.

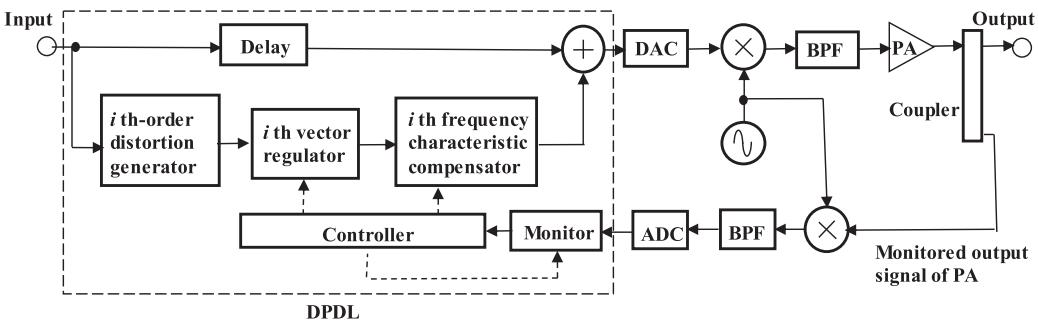

Fig. 8 Basic configuration of DPDL.

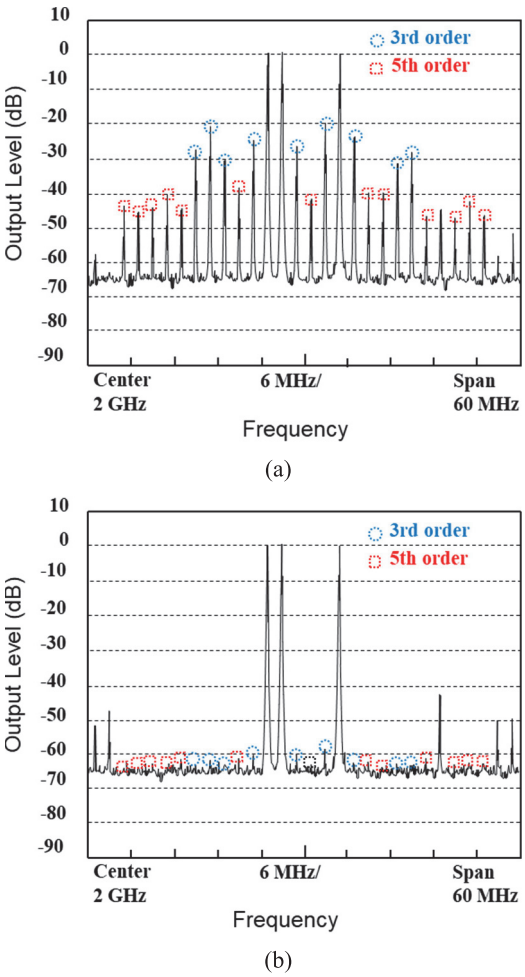

Fig. 10 Experiment results of output spectrum with and without DPDL with frequency characteristic compensator.

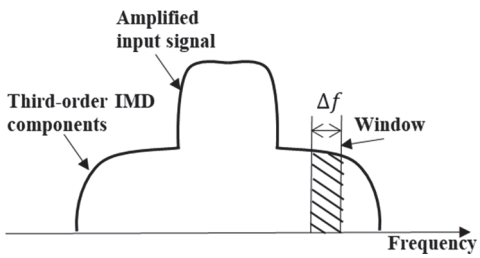

Fig. 11 Spectrum of output signal and window.

Figure 10 (b) shows the output component levels with the DPDL compensating for the frequency dependent components. The DPDL compensates for the third-order and fifth-order IMD components. The frequency characteristic compensators set the optimum amplitude and phase values at each frequency. Figure 10 shows that the DPDL with the frequency characteristic compensators cancels the third-order and fifth-order IMD components generated by the PA.

Figure 11 shows the spectrum of the output signal from the PA. The spectrum level is represented on the vertical axis. The frequency is represented on the horizontal axis.

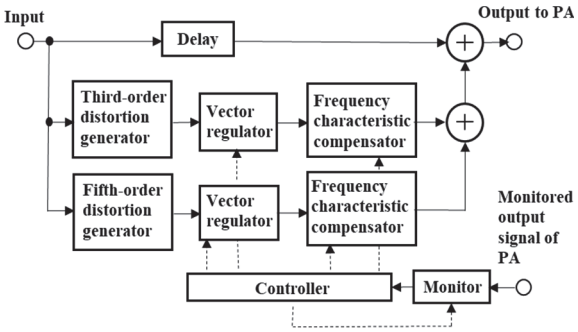

Fig. 12 Configuration of DPDL with frequency characteristic compensator.

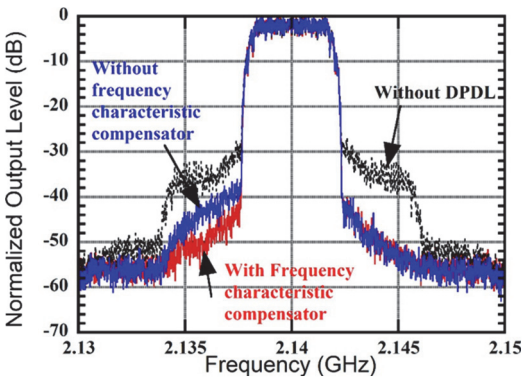

Fig. 13 Output spectrum of PA with DPDL.

The window, Δf, is the bandwidth of the coefficient of the frequency characteristic compensator. The coefficient of the frequency characteristic compensator has the same value in bandwidth Δf. The value of the coefficient is less than 10. This value directly relates to the calculation cost.

3.2 Configuration

Figure 12 shows the DPDL with the frequency characteristic compensator [22]. The DPDL employs commercially available field-programmable gate arrays and digital signal processors. The controller decides the optimum coefficient values of the vector regulator and frequency characteristic compensator [22]. The monitor receives the output signal from the PA, while the monitor selects the desired frequency component with bandwidth Δf. The algorithm for the coefficient setting procedure is the least mean square algorithm [23], but this algorithm requires an enormous calculation cost. In order to reduce the calculation cost, the algorithm that directly calculates the optimum amplitude and phase values using the cube function is presented [24].

3.3 Experimental Results

Figure 13 shows the output spectrum of the PA with and without the DPDL. The output level is represented on the vertical axis. The frequency is represented on the horizontal axis. The test signal is QPSK modulated with the center

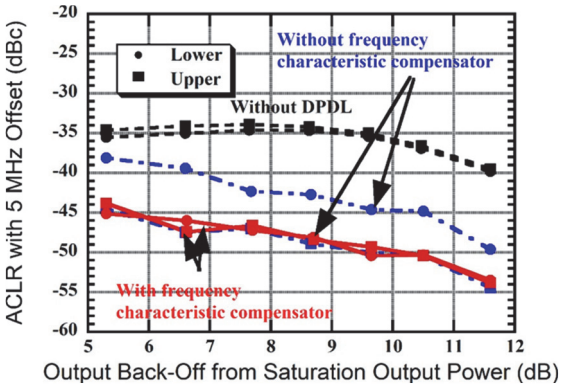

Fig. 14 ACLR performance.

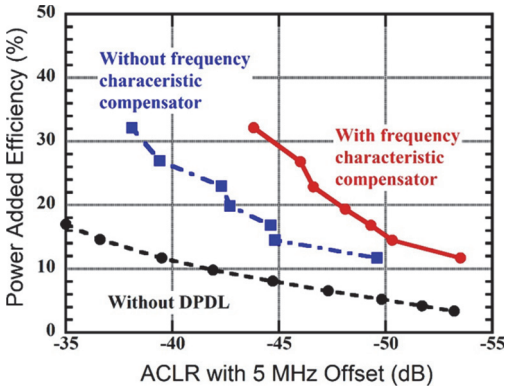

Fig. 15 PAE performance.

frequency of 2.14 GHz and has the bandwidth of 5 MHz. The PA is 1W class using commercially available GaAs MESFETs. The bias condition is set to Class-B. The output back-off level of the PA is 7.6 dB from the saturation output power. The gray line indicates the spectrum of the output signal without the DPDL. The blue line indicates the spectrum of the output signal using the DPDL without the third-order frequency characteristic compensator. The red line represents the spectrum of the output signal using the DPDL with the third-order frequency characteristic compensator. The DPDL without the third-order frequency characteristic compensator has different improvement levels for the lower and upper IMD components. The DPDL with the frequency characteristic compensator can equally achieve the same level for the lower and upper IMD components.

Figure 14 shows the ACLR performance. The ACLR with a 5-MHz offset frequency is represented on the vertical axis. The output back-off from the saturation output power is represented on the horizontal axis. The bias condition, measurement frequency, and test signal are the same as those in Fig. 13. The ACLR without the DPDL is approximately −34 dBc at the output back-off of 8 dB. The lower and upper ACLRs using the DPDL without the frequency characteristic compensator achieve −43 dBc and −46 dBc at the output back-off level of 8 dB, respectively. The DPDL with the frequency characteristic compensator equally achieves lower and upper ACLRs of −47 dBc at the output back-off level of 8 dB. Figure 14 shows that the DPDL with the frequency characteristic compensator can equally compensate the lower and upper IMD components from the output back-off of 5 dB to that of 11.5 dB.

Figure 15 shows the power added efficiency (PAE) performance of the PA. The PAE is represented on the vertical axis. The ACLR with a 5-MHz offset frequency is represented on the horizontal axis. The bias condition, measurement frequency, and test signal are the same as those in Fig. 13. The DPDL with the frequency characteristic compensator achieves the PAE of 28% at the ACLR of −45 dBc, while the DPDL without the frequency characteristic compensator achieves the PAE of 14% at the ACLR of −45 dBc. The PAE of the PA without the DPDL is 8% at the ACLR of −45 dBc. The DPDL with the frequency characteristic compensator improves the PAE by 14 percentage points compared to that for the DPDL without the frequency characteristic compensator. Based on these experimental results, the PA can operate near the saturation output power region.

4. Future Investigation

In general, the FFPA has some advantages such as a superior compensation level and wider compensation bandwidth of the IMD components. On the other hand, the DPDL has some advantages such as a cost effective configuration and lower power consumption. In other words, it can be said that the pros and cons of both are inversely related.

Currently, base station PAs usually employ a DPDL with the Doherty amplifier and compensation scheme of the frequency dependent IMD components regarded as a memory effect. It seems to employ a power series expansion model-based configuration and look-up table configuration for DPDL architectures. Many investigations have been reported. The base station equipment has become smaller and lighter compared to the 2G base station equipment.

The 5G mobile communication systems support radio frequency bands that are lower than the 6-GHz band and millimeter-wave bands such as the 28-GHz band. There are reports regarding the investigations of linearization technologies for millimeter-wave band PAs [25], [26].

One challenge is to compensate for wideband IMD components with frequency dependent IMD components. The third-order IMD components exceed a 1.2-GHz bandwidth if the input signal has a 400-MHz bandwidth. According to Sect. 3.2, the coefficient values also increase in this case. Furthermore, linearization technologies have attained multi-band operation for cellular frequency bands. In this case, complicated IMD components generated by the cellular frequency bands must be compensated [27].

Another challenge is to reduce the power consumption of millimeter-wave band base station equipment. The PA needs to employ a millimeter-wave band power transistor with high linearity and high efficiency. To actualize lower power consumption of the base station equipment, it is in-

dispensable to employ millimeter-wave band power transistors and wideband linearizers. Many research activities have been reported on these topics [28]–[33].

In the future, the DPDL will become main stream in linearization technology for base station PAs. On the other hand, the FFPA will be suitable for wide-band linearization using wide-band modulated signals in the millimeter-wave band.

5. Conclusion

This paper presented linearization technologies for high efficiency PAs in cellular base stations that address the technical issue of high efficiency power amplification with lower non-linear distortion components.

There are two approaches in the investigated linearization technologies, FFPA and DPDL. The first approach is the FFPA with the Doherty amplifier as the main amplifier. This approach reduces the output back-off level of the main amplifier. Therefore, the FFPA with the Doherty amplifier can reduce power consumption while maintaining IMD component levels. The second approach is the DPDL with a frequency characteristic compensator. The frequency characteristic compensator makes a replica of the frequency dependent IMD components. This enables the PA to operate at high efficiency because the frequency dependent IMD components are compensated. The experimental results show the validity of these linearization technologies.

These investigations are fundamental research activities, but we believe that these investigations are the first step toward providing high efficiency PAs in base stations when achieving ACLR specifications. 4G and 5G base station equipment has become more compact and lightweight. Toward the 2030s, new frontier base station PAs will be explored to achieve new technical breakthroughs.

References

[1] ARIB, RCR STD-35, 1993. (*in Japanese*)
[2] ARIB, "Personal digital cellular telecommunication system," RCR STD-27, 1991.
[3] ARIB, "IMT systems based on 3GPP specification," ARIB STD-T120, Sept. 2020.
[4] S. Uebayashi, K. Ohno, and T. Nojima, "Development of TDMA cellular base station equipment," IEEE Proc. Vehicular Tech. Conf., pp.566–569, May 1992.
[5] F.H. Raab, P. Asbeck, S. Cripps, P.B. Kenington, Z.B. Popovic, N. Pothecary, J.F. Sevic, and O. Sokal, "Power amplifiers and transmitters for RF and microwave," IEEE Trans. Microw. Theory Techn., vol.50, no.3, pp.814–826, March 2002.
[6] H. Seidel, "A microwave feed-forward experiment," Bell System Tech. Jour., vol.50, no.9, pp.2789–2916, 1971.
[7] S. Narahashi and T. Nojima, "Extremely low-distortion multi-carrier amplifier – self-adjusting feed-forward (SAFF) amplifier," Proc. IEEE ICC'91, pp.46.5.1–46.5.6, 1991.
[8] Y. Oishi, N. Tozawa, and H. Suzuki, "Highly efficient power amplifier for IMT-2000 BTS equipment," FUJITSHU Sci, Tech. J., vol.38, pp.201–208, Dec. 2002.
[9] H.L. Krauss, C.W. Bostian, and F.H. Raab, Solid State Radio Engineering, John Wiley and Sons, 1980.
[10] S.C. Cripps, RF Power Amplifiers for Wireless Communications, Artech House, 1999.
[11] W.H. Doherty, "A new high efficiency power amplifier for modulated waves," Proc. IRE, vol.24, no.9, pp.1163–1182, 1936.
[12] R.J. McMorrow, D.M. Upton, and P.R. Maloney, "The microwave Doherty amplifier," Proc. IEEE MTT-S Digest, no.TH3E-7, pp.1653–1656, 1994.
[13] S.C. Cripps, Advanced Techniques in RF Power Amplifier Design, Artech House, 2002.
[14] Y. Suzuki, T. Hirota, and T. Nojima, "Highly efficient feed-forward amplifier using a class-F Doherty amplifier," Proc. IEEE MTT-S Int. Microwave Symp. Digest, June 2003.
[15] J.C. Pedro and N.B. Carvalho, Intermodulation Distortion in Microwave and Wireless Circuits, Artech House, 2003.
[16] S.A. Maas, Nonlinear Microwave and RF Circuits, Artech House, 2003.
[17] H. Ku, M.D. McKinley, and J.S. Kenney, "Quantifying memory effect in RF power amplifiers," IEEE Trans. Microw. Theory Techn., vol.50, no.12, pp.2843–2849, Dec. 2002.
[18] N. Pothecary, Feedforward Linear Power Amplifier, Artech House, 1999.
[19] P.B. Kenington, High-Linearity RF Amplifier Design, Artech House, 2000.
[20] S. Nishiki and T. Nojima, "Harmonic reaction amplifier – A novel high efficiency and high power microwave amplifier –," Proc. IEEE MTT-S Int. Microwave Symp. Digest, vol.DD-5, pp.963–966, 1987.
[21] S. Mizuta, Y. Suzuki, T. Hirota, and Y. Yamao, "Digital predistortion linearizer for compensating frequency-dependent IM distortion," Proc. 34th European Microwave Conference, Amsterdam, The Netherlands, pp.1053–1056, Oct. 2004.
[22] S. Mizuta, Y. Suzuki, S. Narahashi, and Y. Yamao, "A new adjustment method for the frequency-dependent IMD compensator of the digital predistortion linearizer," Proc. 2006 IEEE Radio and Wireless Symp., Oct. 2006.
[23] S. Haykin, Adaptive Filter Theory third edition, Prentice-Hall, 1996.
[24] J. Ohkawara, Y. Suzuki, and S. Narahashi, "Fast calculation scheme for frequency characteristic IMD compensator of digital predistortion linearizer," Proc. IEEE 69th Vehicular Tech. Conf., April 2009.
[25] K. Kunihiro, S. Hori, and T. Kaneko, "High efficiency power amplifiers for mobile base stations: Recent trends and future prospects for 5G," IEICE Trans. Fundamentals, vol.E101-A, no.2, pp.374–384, Feb. 2018.
[26] S. Tanaka, "Progress of the linear RF power amplifier for mobile phones," IEICE Trans. Fundamentals, vol.E101-A, no.2, pp.385–395, Feb. 2018.
[27] Y. Suzuki, H. Okazaki, and S. Narahashi, "IMD components compensation Conditions for dual-band feed-forward power amplifier," IEICE Trans. Electron., vol.E103-C, no.10, pp.434–444, Oct. 2020.
[28] A. Katz, J. Wood, and D. Chokola, "The evolution of PA linearization: From classic feedforward and feedback through analog and digital predistortion," IEEE Microw. Mag., vol.17, no.2, pp.32–40, Jan. 2016.
[29] P.L. Gilabert, G. Montoro, D. Vegas, N. Ruiz, and J.A. Garcia, "Digital predistorters go multidimensional: DPD for concurrent multiband envelope tracking and outphasing power amplifiers," IEEE Microw. Mag., vol.20, no.5, pp.50–61, April 2019.
[30] H. Nakamizo, S. Shinjo, K. Tsutsumi, S. Yamaguchi, H. Yoshioka, A. Okazaki, A. Taira, and K. Tajima, "A compact RF frontend module of active phased array antenna for high SHF wideband massive MIMO in 5G," IEICE Trans. Electron., vol.E100-C, no.10, pp.818–824, Oct. 2017.
[31] Z. Popovic, "Amping up the PA for 5G: Efficient GaN power amplifiers with dynamic supplies," IEEE Microw. Mag., vol.18, no.3, pp.137–149, May 2017.
[32] T. Qi and S. He, "Power up potential power amplifier technologies for 5G applications," IEEE Microw. Mag., vol.20, no.6, pp.89–101, May 2019.
[33] K. Miyanaga, M. Kobayashi, N. Saito, N. Shirakata, and K.

Takinami, "A wideband asymmetric digital predistortion architecture for 60 GHz short range wireless transmitters," IEICE Trans. Electron., vol.E99-C, no.10, pp.1190–1199, Oct. 2016.

Yasunori Suzuki received the B.E. and M.E. degrees from Nagaoka University of Technology, Niigata, Japan, in 1993 and 1995, respectively, and the Ph.D. degree from Hokkaido University, Sapporo, Japan, in 2011. In 1995, he joined NTT Mobile Communications Network, Inc. (now NTT DOCOMO, INC.) where he was engaged in research on base station equipment for mobile communications. He is currently a Senior Manager of 6G Laboratories. He is a senior member of the IEICE. He is a member of the IEEE.

Shoichi Narahashi received the B.E. and M.E. degrees from Kumamoto University, Kumamoto, Japan, in 1986 and 1988, respectively, and the Ph.D. degree from Hokkaido University, Sapporo, Japan, in 2008. In 1988, he joined the Radio Communication Systems Laboratories, Nippon Telegraph and Telephone (NTT) Corporation where he was engaged in research and development on base station equipment for digital mobile communications. From 1992 to 2017, he was with NTT DOCOMO, INC, where he was an Executive Research Engineer with the mission of investigating RF technologies for mobile communications. He is currently a Professor of the Faculty of Science and Engineering, Setsunan University. He was the recipient of the 2011 IEICE Achievement Award and the 2012 IEICE Best Paper Award. He is a member of the IEEE and the Institute of Electrical Engineers of Japan (IEEJ).